EXPLAINING EXTREME EVENTS OF 2016

From A Climate Perspective

Special Supplement to the
Bulletin of the American Meteorological Society
Vol. 99, No. 1, January 2018

EXPLAINING EXTREME EVENTS OF 2016 FROM A CLIMATE PERSPECTIVE

Editors

Stephanie C. Herring, Nikolaos Christidis, Andrew Hoell, James P. Kossin, Carl J. Schreck III, and Peter A. Stott

Special Supplement to the

Bulletin of the American Meteorological Society

Vol. 99, No. 1, January 2018

AMERICAN METEOROLOGICAL SOCIETY

Corresponding Editor:

Stephanie C. Herring, PhD
NOAA National Centers for Environmental Information
325 Broadway, E/CC23, Rm 1B-131
Boulder, CO 80305-3328
E-mail: stephanie.herring@noaa.gov

Cover credit:

©The Ocean Agency / XL Catlin Seaview Survey / Chrisophe Bailhache—A panoramic image of coral bleaching at Lizard Island on the Great Barrier Reef, captured by The Ocean Agency / XL Catlin Seaview Survey / Christophe Bailhache in March 2016.

HOW TO CITE THIS DOCUMENT

Citing the complete report:

Herring, S. C., N. Christidis, A. Hoell, J. P. Kossin, C. J. Schreck III, and P. A. Stott, Eds., 2018: Explaining Extreme Events of 2016 from a Climate Perspective. *Bull. Amer. Meteor. Soc.*, **99** (1), S1–S157.

Citing a section (example):

Quan, X.W., M. Hoerling, L. Smith, J. Perlwitz, T. Zhang, A. Hoell, K. Wolter, and J. Eischeid, 2018: Extreme California Rains During Winter 2015/16: A Change in El Niño Teleconnection? [in "Explaining Extreme Events of 2016 from a Climate Perspective"]. *Bull. Amer. Meteor. Soc.*, **99** (1), S54–S59, doi:10.1175/BAMS-D-17-0118.1.

EDITORIAL AND PRODUCTION TEAM

Riddle, Deborah B., Lead Graphics Production, NOAA/NESDIS National Centers for Environmental Information, Asheville, NC

Love-Brotak, S. Elizabeth, Graphics Support, NOAA/NESDIS National Centers for Environmental Information, Asheville, NC

Veasey, Sara W., Visual Communications Team Lead, NOAA/NESDIS National Centers for Environmental Information, Asheville, NC

Fulford, Jennifer, Editorial Support, Telesolv Consulting LLC, NOAA/NESDIS National Centers for Environmental Information, Asheville, NC

Griffin, Jessicca, Graphics Support, Cooperative Institute for Climate and Satellites-NC, North Carolina State University, Asheville, NC

Misch, Deborah J., Graphics Support, Telesolv Consulting LLC, NOAA/NESDIS National Centers for Environmental Information, Asheville, NC

Osborne, Susan, Editorial Support, Telesolv Consulting LLC, NOAA/NESDIS National Centers for Environmental Information, Asheville, NC

Sprain, Mara, Editorial Support, LAC Group, NOAA/NESDIS National Centers for Environmental Information, Asheville, NC

Young, Teresa, Graphics Support, Telesolv Consulting LLC, NOAA/NESDIS National Centers for Environmental Information, Asheville, NC

TABLE OF CONTENTS

ABSTRACT—Stephanie C. Herring, Nikolaos Christidi, Andrew Hoell, James P. Kossin, Carl J. Schreck III, and Peter A. Stott

This sixth edition of explaining extreme events of the previous year (2016) from a climate perspective is the first of these reports to find that some extreme events were not possible in a preindustrial climate. The events were the 2016 record global heat, the heat across Asia, as well as a marine heat wave off the coast of Alaska. While these results are novel, they were not unexpected. Climate attribution scientists have been predicting that eventually the influence of human-caused climate change would become sufficiently strong as to push events beyond the bounds of natural variability alone. It was also predicted that we would first observe this phenomenon for heat events where the climate change influence is most pronounced. Additional retrospective analysis will reveal if, in fact, these are the first events of their kind or were simply some of the first to be discovered.

Last year, the editors emphasized the need for additional papers in the area of "impacts attribution" that investigate whether climate change's influence on the extreme event can subsequently be directly tied to a change in risk of the socio-economic or environmental impacts. Several papers in this year's report address this challenge, including Great Barrier Reef bleaching, living marine resources in the Pacific, and ecosystem productivity on the Iberian Peninsula. This is an increase over the number of impact attribution papers than in the past, and are hopefully a sign that research in this area will continue to expand in the future.

Other extreme weather event types in this year's edition include ocean heat waves, forest fires, snow storms, and frost, as well as heavy precipitation, drought, and extreme heat and cold events over land. There were a number of marine heat waves examined in this year's report, and all but one found a role for climate change in increasing the severity of the events. While human-caused climate change caused China's cold winter to be less likely, it did not influence U.S. storm Jonas which hit the mid-Atlantic in winter 2016.

As in past years, the papers submitted to this report are selected prior to knowing the final results of whether human-caused climate change influenced the event. The editors have and will continue to support the publication of papers that find no role for human-caused climate change because of their scientific value in both assessing attribution methodologies and in enhancing our understanding of how climate change is, and is not, impacting extremes. In this report, twenty-one of the twenty-seven papers in this edition identified climate change as a significant driver of an event, while six did not. Of the 131 papers now examined in this report over the last six years, approximately 65% have identified a role for climate change, while about 35% have not found an appreciable effect.

Looking ahead, we hope to continue to see improvements in how we assess the influence of human-induced climate change on extremes and the continued inclusion of stakeholder needs to inform the growth of the field and how the results can be applied in decision making. While it represents a considerable challenge to provide robust results that are clearly communicated for stakeholders to use as part of their decision-making processes, these annual reports are increasingly showing their potential to help meet such growing needs.

22. DO CLIMATE CHANGE AND EL NIÑO INCREASE LIKELIHOOD OF YANGTZE RIVER EXTREME RAINFALL?

Xing Yuan, Shanshan Wang, and Zeng-Zhen Hu

Anthropogenic climate change has increased the risk of 2016 Yangtze River extreme summer rainfall by 17%–59%, and the increase could reach 37%–91% in El Niño years.

Introduction. In June–July 2016, a barrage of extreme rainfall hit the middle and lower reaches of Yangtze River in eastern China, which caused severe urban inundations in large cities such as Wuhan and Nanjing, and resulted in direct economic loss of 70 billion RMB (about $10 billion U.S. dollars). Similar to the 1998 Yangtze River extreme rainfall, the 2016 extreme rainfall coincided with the decaying phase of 2015/16 super El Niño through Pacific–East Asian teleconnection which enhanced the west Pacific subtropical high (WPSH) and weakened the East Asia summer monsoon (EASM), resulting in an anomalously anticyclonic circulation pattern over the northwestern Pacific that brought lots of atmospheric moisture from the Pacific to the Yangtze River (Wang et al. 2000; Yuan et al. 2017). A possible mechanism for the lag-impact of El Niño/Southern Oscillation (ENSO) on East Asia summer climate is the Indo–western Pacific Ocean capacitor (IPOC), where the North Indian Ocean warming after El Niño plays an important role (Xie et al. 2016). The spatial distribution of the 2016 extreme rainfall, however, is different from that in 1998 with a northward shift of the ENSO-forced teleconnection (Figs. 22.1e,f), which raises the question of whether the climate change and El Niño increase the likelihood of Yangtze River extreme rainfall. This paper will examine the 2016 extreme rainfall in a historical context, and investigate the effects of anthropogenic climate change and natural climate variability (e.g., ENSO) on the likelihood of the extreme rainfall.

AFFILIATIONS: Yuan—Key Laboratory of Regional Climate-Environment for Temperate East Asia, Institute of Atmospheric Physics, Chinese Academy of Sciences, Beijing, China; Wang—Key Laboratory of Arid Climatic Change and Reducing Disaster of Gansu Province, and Key Open Laboratory of Arid Climate Change and Disaster Reduction of CMA, Institute of Arid Meteorology, CMA, Lanzhou, China; Hu—NOAA/NWS/NCEP Climate Prediction Center, College Park, Maryland

DOI:10.1175/BAMS-D-17-0089.1

A supplement to this article is available online (10.1175/BAMS-D-17-0089.2)

Data and methods. Daily rainfall observations from 2474 China Meteorological Administration (CMA) stations provided by CMA National Meteorological Information Center (NMIC) were interpolated into 0.25-degree grid cells during June–July of 1951–2016 by using the inverse quadratic distance weighting method (Yuan et al. 2016). Detecting the human influence on precipitation change is a grand challenge especially at regional or local scales (Hu et al. 2003; Zhang et al. 2007). Therefore, daily rainfall at 0.25-degree grid cells were averaged over the middle and lower reaches of Yangtze River (27°–34°N, 110°–123°E) for a more robust analysis. The area-averaged maximum 10-day rainfall amounts (RX10day) during each June–July, which is a good indicator for flooding, was selected to represent the extreme rainfall over Yangtze River. The generalized extreme value (GEV) distribution was used to fit the extreme rainfall distribution and to estimate the return period in this study.

To analyze the ENSO impact on the extreme rainfall, the extended reconstructed sea surface temperature version 4 (ERSSTv4; Huang et al. 2014) monthly data during 1854–2016 was used as SST observations in this study. An El Niño event was defined as the mean Niño-3.4 (5°S–5°N, 120°–170°W) SST anomaly during preceding December–February (DJF) exceeding 0.95°C (1σ) of the Niño-3.4 SST time series; a La Niña event was defined by a mean SST anomaly of less than −0.95°C. Note that the same criterion (> 0.95°C) was also applied for the model simulations for the ENSO identification.

Daily rainfall and SST simulations from 14 atmosphere–ocean coupled general circulation models (CGCMs; see Table ES22.1 for the model list) provided by the Coupled Model Intercomparison Project Phase

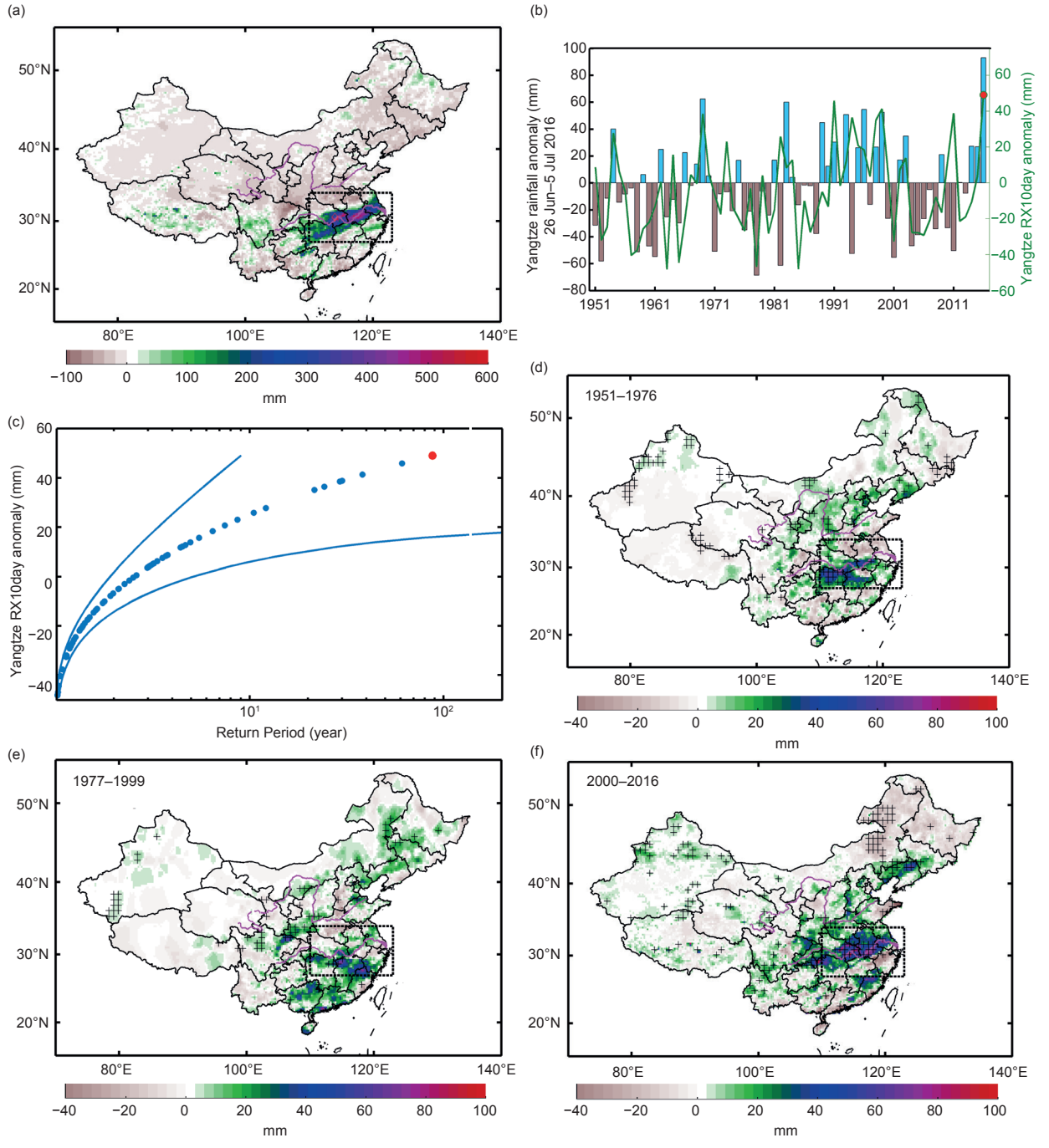

Fig. 22.1. (a) Rainfall anomaly (colors; mm) in 26 Jun–5 Jul 2016 relative to 1981–2010 climatology in CMA/NMIC observations. (b) Time series of 10-day accumulated rainfall anomaly (bar plot; mm) of 26 Jun–5 Jul averaged over middle and lower reaches of Yangtze River [27°–34°N, 110°–123°E; dashed box in (a)] and Yangtze River RX10day anomaly during Jun–Jul (green line; mm). (c) Return period (years) and 95% CI for RX10day anomaly; red dot represents 2016. (d)–(f) Regressed RX10day anomaly (colors; mm) against Niño-3.4 SST in the preceding DJF during 1951–76, 1977–99, and 2000–16, respectively; stippling indicates a 90% confidence level ($p < 0.1$).

5 (CMIP5; Taylor et al. 2012) were used in this study. For each CGCM, several pairs of realizations driven by all (ALL) and natural only (NAT) forcings during 1950–2005 were used. A number of evaluation tests were carried out to identify models: 1) as compared with observation, variability of both simulated consecutive 10-day rainfall averaged over middle and lower Yangtze River and DJF Niño-3.4 SST should pass the Kolmogorov–Smirnov test with $p < 0.05$; 2) standard deviations of model simulated Niño-3.4 SST

should be less than 1.43°C (1.5σ of observed Niño-3.4 SST); and 3) both ALL and NAT experiments should produce a positive correlation between DJF Niño-3.4 and June–July RX10day. After evaluation, six CMIP5 models with 12 realizations (red bold in Table ES22.1) were selected to determine the effects of anthropogenic climate change and ENSO on the Yangtze River extreme rainfall. The fraction of attributable risk (FAR; Stott et al. 2004) method that compares the event tail probabilities (P) between CMIP5/NAT and CMIP5/ALL simulations ($FAR = 1-P_{NAT}/P_{ALL}$), was used to assess the contribution of anthropogenic climate change. For instance, a value of FAR = 0.5 suggests that the risk of an extreme event is doubled over natural conditions due to anthropogenic climate change. Bootstrapping was performed 1000 times to estimate the FAR uncertainty.

Results. Figure 22.1a shows the spatial distribution of 10-day accumulated rainfall anomaly during 26 June–5 July in 2016. Extreme rainfall was found to have occurred over the middle and lower reaches of Yangtze River, with anomaly exceeding 300–400 mm within 10 days. Moreover, the area-averaged 10-day rainfall anomaly in 2016 is ranked as the first during recent 66 years (1951–2016) according to the CMA/NMIC observations (bar plot in Fig. 22.1b). Figure 22.1c shows that the RX10day extreme rainfall index in 2016 is also ranked as the first during 1951–2016, with a return period of 88 years (>8 years at 95% confidence level).

The Yangtze River extreme rainfall occurred in the context of the 2015/16 super El Niño. Actually there were statistically significant correlations between Yangtze River extreme summer rainfall and preceding Niño-3.4 index. Figure ES22.1 shows that the RX10day index during summer positively correlated with the Niño-3.4 index in the preceding cold seasons, with the highest correlation for DJF Niño-3.4 index. To assess the El Niño impacts spatially, the RX10day at each 0.25-degree grid cell were regressed against Niño-3.4 index during preceding DJF (Wu et al. 2003). Figures 22.1d–f show the regressed RX10day for the periods of 1951–76, 1977–99, and 2000–16, respectively, where the ENSO forced teleconnection pattern shifts from southeastern China to the middle and lower reaches of Yangtze River after 2000, resulting in a pattern (Fig. 22.1f) that is similar to the 2016 extreme rainfall (Fig. 22.1a). This suggests the northward shift of the ENSO forced teleconnection may increase the risk of extreme rainfall over Yangtze River. The cause of the shift is still unclear, and one possibility is the decadal internal variability, such as interdecadal Pacific oscillation (IPO). For example, Song and Zhou (2016) found that the IPO plays a dominant role in the decadal variation of the relationship between ENSO and East Asian summer monsoon during the twentieth century.

Figure ES22.1 also shows that although the correlation is statistically significant, it is actually very weak (less than 0.25). This implies that other factors, such as sea–ice, land surface processes, stratosphere, and unforced internal variability due to the chaos of the weather, may play a role. Moreover, Gao et al. (2014) argued that only a small fraction of monthly precipitation in eastern China is predictable. He et al. (2016) also indicated that only about 18% of the interannual variation of rainfall over East Asian land can be explained by SST. Tropical Indian and Pacific Oceans each account for approximately 6% of the total variance of rainfall. These studies document the dominant role of atmospheric internal dynamical processes in variation of East Asian summer rainfall. In fact, Sterl et al. (2007) showed that changes in the strength of ENSO teleconnection could be very small and only detectable on centennial time scales.

To explore the causality of the risk change, CMIP5 model simulations with ALL and NAT-only forcings were used. Similar to other CGCM applications (Yuan and Wood 2013; Wang et al. 2017), CMIP5 models seem to overrepresent the ENSO–seasonal mean rainfall teleconnection (not shown) and under-represent the ENSO–extreme rainfall teleconnection (Fig. ES22.2). Models' simulations on the teleconnection pattern, however, can be improved to some extent with the consideration of anthropogenic forcings (Fig. ES22.2), suggesting that anthropogenic climate change may play an important role in influencing the likelihood of the Yangtze River extreme rainfall.

Therefore, the probability density functions (PDFs) for RX10day of CMIP5 model simulations, were calculated by fitting GEV distributions. The FAR for the RX10day heavier than the 2016 case is 0.38 (±0.21), with the return period decreased from 72 years [95% confidence interval (CI): 34–238 years] to 45 years (CI: 24–120 years) under the influence of the anthropogenic climate change (Fig. 22.2a). For the results during El Niño years (Fig. 22.2b), there is a more robust difference between the simulations with and without anthropogenic forcings, with FAR changed to 0.64 (±0.27). Figure 22.2b also shows that an extreme rainfall event like that in 2016 is most likely to occur in El Niño years with ALL forcings (red square), and least likely in La Niña years without

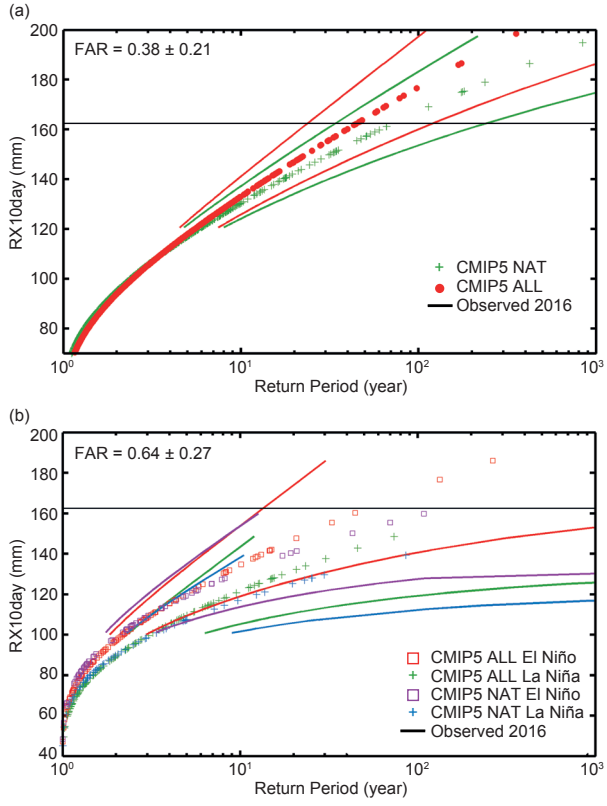

Fig. 22.2. (a) Return periods for Yangtze River RX10day anomaly from CMIP5 simulations under ALL and NAT forcings during 1950–2005. (b) As in (a), but during El Niño or La Niña years (see text for definitions).

anthropogenic forcings (blue plus). The results for El Niño years without anthropogenic forcings (purple square) and La Niña years with all forcings (green plus) are between them. Under ALL forcing conditions, El Niño years increase the likelihood of having extreme rainfall from La Niña years by 416% (±200%).

Conclusions. Extreme rainfall hit the middle and lower reaches of Yangtze River during the summer of 2016, where the anomaly exceeded 300–400 mm within 10 days, ranking as the heaviest 10-day rainfall since 1951. In fact, the observed ENSO-extreme rainfall teleconnection shows a northward shift after 2000 and may increase the risk of extreme rainfall over the Yangtze River, although such northward shift of the teleconnection is compatible with natural variability. By using CMIP5 model simulations, it is found that the likelihood of Yangtze River extreme rainfall such as that occurring in 2016 has increased by about 38% (±21%) due to anthropogenic climate change, and the likelihood can be increased by 64% (±27%) in El Niño years. There are large uncertainties, however, both because of complicated causes of Yangtze River extreme rainfall, and the deficiencies in current CMIP5 models in representing ENSO, ENSO-teleconnection, and extreme rainfall processes.

ACKNOWLEDGMENTS. We would like to thank Dr. Martin Hoerling, Dr. James Kossin, and three anonymous reviewers for their constructive comments. We acknowledge the World Climate Research Programme's Working Group on Coupled Modeling, which is responsible for CMIP. This work was supported by National Natural Science Foundation of China (91547103, 41605055), National Key R&D Program of China (2016YFA0600403), and Thousand Talents Program for Distinguished Young Scholars.

REFERENCES

Gao, Z., Z.-Z. Hu, B. Jha, S. Yang, J. Zhu, B. Shen, and R. Zhang, 2014: Variability and predictability of Northeast China climate during 1948–2012. *Climate Dyn.*, **43**, 787–804, doi:10.1007/s00382-013-1944-0.

He, C., B. Wu, C. Li, A. Lin, D. Gu, Z. Zheng, and T. Zhou, 2016: How much of the interannual variability of East Asian summer rainfall is forced by SST? *Climate Dyn.*, **47**, 555–565, doi:10.1007/s00382-015-2855-z.

Hu, Z.-Z., S. Yang, and R. Wu, 2003: Long-term climate variations in China and global warming signals. *J. Geophys. Res.*, **108**, 4614, doi:10.1029/2003JD003651.

Huang, B., and Coauthors, 2014: Extended reconstructed sea surface temperature version 4 (ERSST.v4): Part I. Upgrades and intercomparisons. *J. Climate*, **28**, 911–930, doi:10.1175/JCLI-D-14-00006.1.

Song, F., and T. Zhou, 2015: The crucial role of internal variability in modulating the decadal variation of the East Asian summer monsoon–ENSO relationship during twentieth century. *J. Climate*, **28**, 7093–7107, doi:10.1175/JCLI-D-14-00783.1.

Sterl, A., G. J. van Oldenborgh, W. Hazeleger, and G. Burgers, 2007: On the robustness of ENSO teleconnections. *Climate Dyn.*, **29**, 469–485, doi:10.1007/s00382-007-0251-z/.

Stott, P. A., D. A. Stone, and M. R. Allen, 2004: Human contribution to the European heatwave of 2003. *Nature*, **432**, 610–614, doi:10.1038/nature03089.

Taylor, K. E., R. J. Stouffer, and G. A. Meehl, 2012: An overview of CMIP5 and the experiment design. *Bull. Amer. Meteor. Soc.*, **93**, 485–498, doi:10.1175/BAMS-D-00094.1.

Wang, B., R. Wu, and X. Fu, 2000: Pacific–East Asian teleconnection: How does ENSO affect East Asian climate? *J. Climate*, **13**, 1517–1536, doi:10.1175/1520-0442(2000)013<1517:PEATHD>2.0.CO;2.

Wang, S., X. Yuan, and Y. Li, 2017: Does a strong El Niño imply a higher predictability of extreme drought? *Sci. Rep.*, **7**, 40741, doi:10.1038/srep40741.

Wu, R., Z.-Z. Hu, and B. P. Kirtman, 2003: Evolution of ENSO-related rainfall anomalies in East Asia. *J. Climate*, **16**, 3742–3758, doi:10.1175/1520-0442(2003)016<3742:EOERAI>2.0.CO;2.

Xie, S.-P., Y. Kosaka, Y. Du, K. Hu, J. S. Chowdary, and G. Huang, 2016: Indo–western Pacific Ocean capacitor and coherent climate anomalies in post-ENSO summer: A review. *Adv. Atmos. Sci.*, **33**, 411–432, doi:10.1007/s00376-015-5192-6.

Yuan, X., and E. F. Wood, 2013: Multimodel seasonal forecasting of global drought onset. *Geophys. Res. Lett.*, 40, 4900–4905, doi:10.1002/grl.50949.

——, F. Ma, L. Wang, Z. Zheng, Z. Ma, A. Ye, and S. Peng, 2016: An experimental seasonal hydrological forecasting system over the Yellow River basin-Part 1: Understanding the role of initial hydrological conditions. *Hydrol. Earth Syst. Sci.*, **20**, 2437–2451, doi:10.5194/hess-20-2437-2016.

Yuan, Y., H. Gao, W. Li, Y. Liu, L. Chen, B. Zhou, and Y. Ding, 2017: The 2016 summer floods in China and associated physical mechanisms: A comparison with 1998. *J. Meteor. Res.*, **31**, 216–277, doi:10.1007/s13351-017-6192-5.

Zhang, X., F. W. Zwiers, G. C. Hegerl, F. H. Lambert, N. P. Gillett, S. Solomon, P. A. Stott, and T. Nozawa, 2007: Detection of human influence on twentieth-century precipitation trends. *Nature*, **448**, 461–466, doi:10.1038/nature06025.

Table 1.1. SUMMARY of RESULTS

ANTHROPOGENIC INFLUENCE ON EVENT			
	INCREASE	**DECREASE**	**NOT FOUND OR UNCERTAIN**
Heat	Ch. 3: Global Ch. 7: Arctic Ch. 15: France Ch. 19: Asia		
Cold		Ch. 23: China Ch. 24: China	
Heat & Dryness	Ch. 25: Thailand		
Marine Heat	Ch. 4: Central Equatorial Pacific Ch. 5: Central Equatorial Pacific Ch. 6: Pacific Northwest Ch. 8: North Pacific Ocean/Alaska Ch. 9: North Pacific Ocean/Alaska Ch. 9: Australia		Ch. 4: Eastern Equatorial Pacific
Heavy Precipitation	Ch. 20: South China Ch. 21: China (Wuhan) Ch. 22: China (Yangtze River)		Ch. 10: California (failed rains) Ch. 26: Australia Ch. 27: Australia
Frost	Ch. 29: Australia		
Winter Storm			Ch. 11: Mid-Atlantic U.S. Storm "Jonas"
Drought	Ch. 17: Southern Africa Ch. 18: Southern Africa		Ch. 13: Brazil
Atmospheric Circulation			Ch. 15: Europe
Stagnant Air			Ch. 14: Western Europe
Wildfires	Ch. 12: Canada & Australia (Vapor Pressure Deficits)		
Coral Bleaching	Ch. 5: Central Equatorial Pacific Ch. 28: Great Barrier Reef		
Ecosystem Function		Ch. 5: Central Equatorial Pacific (Chl-***a*** and primary production, sea bird abundance, reef fish abundance) Ch. 18: Southern Africa (Crop Yields)	
El Niño	Ch. 18: Southern Africa		Ch. 4: Equatorial Pacific (Amplitude)
TOTAL	18	3	9

	METHOD USED	Total Events
Heat	Ch. 3: CMIP5 multimodel coupled model assessment with piCont, historicalNat, and historical forcings Ch. 7: CMIP5 multimodel coupled model assessment with piCont, historicalNat, and historical forcings Ch. 15: Flow analogues conditional on circulation types Ch. 19: MIROC-AGCM atmosphere only model conditioned on SST patterns	
Cold	Ch. 23: HadGEM3-A (GA6) atmosphere only model conditioned on SST and SIC for 2016 and data fitted to GEV distribution Ch. 24: CMIP5 multimodel coupled model assessment	
Heat & Dryness	Ch. 25: HadGEM3-A N216 Atmosphere only model conditioned on SST patterns	
Marine Heat	Ch. 4: SST observations; SGS and GEV distributions; modeling with LIM and CGCMs (NCAR CESM-LE and GFDL FLOR-FA) Ch. 5: Observational extrapolation (OISST, HadISST, ERSST v4) Ch. 6: Observational extrapolation; CMIP5 multimodel coupled model assessment Ch. 8: Observational extrapolation; CMIP5 multimodel coupled model assessment Ch. 9: Observational extrapolation; CMIP5 multimodel coupled model assessment	
Heavy Precipitation	Ch. 10: CAM5 AMIP atmosphere only model conditioned on SST patterns and CESM1 CMIP single coupled model assessment Ch. 20: Observational extrapolation; CMIP5 and CESM multimodel coupled model assessment; auto-regressive models Ch. 21: Observational extrapolation; HadGEM3-A atmosphere only model conditioned on SST patterns; CMIP5 multimodel coupled model assessment with ROF Ch. 22: Observational extrapolation, CMIP5 multimodel coupled model assessment Ch. 26: BoM seasonal forecast attribution system and seasonal forecasts Ch. 27: CMIP5 multimodel coupled model assessment	
Frost	Ch. 29: *weather@home* multimodel atmosphere only models conditioned on SST patterns; BoM seasonal forecast attribution system	
Winter Storm	Ch. 11: ECHAM5 atmosphere only model conditioned on SST patterns	
Drought	Ch. 13: Observational extrapolation; weather@home multimodel atmosphere only models conditioned on SST patterns; HadGEM3-A and CMIP5 multimodel coupled model assessent; hydrological modeling Ch. 17: Observational extrapolation; CMIP5 multimodel coupled model assessment; VIC land surface hdyrological model, optimal fingerprint method Ch. 18: Observational extrapolation; *weather@home* multimodel atmosphere only models conditioned on SSTs, CMIP5 multimodel coupled model assessment	
Atmospheric Circulation	Ch. 15: Flow analogues distances analysis conditioned on circulation types	
Stagnant Air	Ch. 14: Observational extrapolation; Multimodel atmosphere only models conditioned on SST patterns including: HadGEM3-A model; EURO-CORDEX ensemble; EC-EARTH+RACMO ensemble	
Wildfires	Ch. 12: HadAM3 atmospere only model conditioned on SSTs and SIC for 2015/16	
Coral Bleaching	Ch. 5: Observations from NOAA Pacific Reef Assessment and Monitoring Program surveys Ch. 28: CMIP5 multimodel coupled model assessment; Observations of climatic and environmental conditions (NASA GES DISC, HadCRUT4, NOAA OISSTV2)	
Ecosystem Function	Ch. 5: Observations of reef fish from NOAA Pacific Reef Assessment and Monitoring Program surveys; visual observations of seabirds from USFWS surveys. Ch. 18: Empirical yield/rainfall model	
El Niño	Ch. 4: SST observations; SGS and GEV distributions; modeling with LIM and CGCMs (NCAR CESM-LE and GFDL FLOR-FA) Ch. 18: Observational extrapolation; *weather@home* multimodel atmosphere only models conditioned on SSTs, CMIP5 multimodel coupled model assessment	
		30